KRONOS FUSION ENERGY

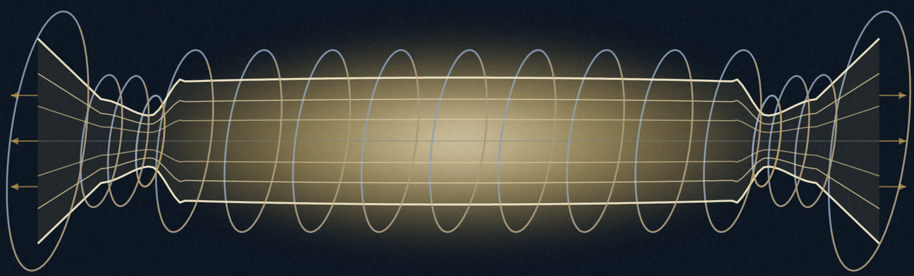

PAPER 2.57 · THE KRONOS 2026 SERIES

Sloshing-Ion Ambipolar-Potential Formation in a D–^{3}He Tandem-Mirror Burner: The Density-Ratio–Potential Pareto and Non-Maxwellian Tail Control

The engineering gain of a D–He tandem-mirror burner is set, through an exponential Pastukhov confinement law, by the ambipolar potential that its high-field end plug can hold;...

Read it live — 3-D model · physics validator · film series

BY P I FORD AND G L KULCINSKI

2026 · EDITORIAL EDITION

THE OFFICIAL RECORD

What this document is, and how to read its numbers

This is a combined editorial. It gathers, in one volume, the two design studies Kronos Fusion Energy released in 2026 — a compact spherical-tokamak tritium/helium-3 breeder and a deuterium–helium-3 tandem-mirror generator — together with the intellectual-property estate, the people, and, in the internal edition, the full commercial case. The scientific text is the same text that appears in the arXiv preprints and the journal submissions; the editorial adds the apparatus a reader needs to hold the whole program at once, and nothing in the physics is altered to fit it.

THE HONESTY STANCE IS THE ASSET

Every headline quantity carries an **evidence class** — DERIVED RECOMPUTED MEASURED REQUIREMENT — and, where a number is a modelled extrapolation rather than a demonstrated value, it is labelled as such and its downside is shown next to it. Several quantities in the underlying corpus moved after first publication; where a value has been withdrawn or restated, the record says so plainly. This is deliberate: a diligence team will find the load-bearing assumptions, so the document surfaces them first.

TWO EDITIONS

This volume is issued in two editions. The **public edition** (light) carries the physics and the design only — no dollar, price, or per-kilogram figure appears anywhere in it. The **internal edition** (dark) adds the economics, the funding architecture, and the defense-commercial analysis, and is marked *Confidential* accordingly; it is not for public distribution. Where the commercial case rests on a modelled assumption rather than a demonstrated one, it is labelled as such and its downside is shown alongside it, on the same terms as the physics.

TITLE	The Kronos Fleet — Hyperion · Aegis · MetroVolt: A Combined Design & Commercialization Study
AUTHOR	Priyanca Ford, Founder & CEO, on behalf of Kronos Fusion Energy
EDITION	2026 Combined Editorial · first issue
COMPANION WORKS	The five-paper arXiv drop — (1) Breeder, (2) Burner, (3) REBCO magnet & tape, (4) Direct Energy Conversion, (5) AI/ML/Quantum control — with matching numbered Zenodo deposits, plus the IOP journal and IAEA-FEC submissions. Patents were filed before the drop.
NAMING	Hyperion = the breeder; Aegis (defense) and MetroVolt (data-center) = one generator in two housings. Internal mode letters (D1, L) do not appear on public surfaces.
STATUS	Conceptual design & simulation study. Nothing herein is a construction commitment.

HOW TO READ THIS VOLUME

The fleet at a glance, and the way its numbers are marked

This volume opens with *Orientation*, presents the five research papers as a bound sequence, and closes with the *Apparatus*. *Foundations* sets out the three general results both machines rest on. *Paper One* is the Hyperion breeder; *Paper Two* the Aegis / MetroVolt generator; *Papers Three, Four and Five* are the enabling science — high-field REBCO magnets and tape, direct energy conversion, and the AI / ML / quantum control stack. A *Digital Twin & 3-D Model* part follows, then the *Environmental* profile. The *Economics* and levelized cost and the *Business Case* and diligence record appear in the internal edition only; the *Simulations* proof record and the Apparatus — patent portfolio, team, limitations, and sources — close both editions.

THE FLEET AT A GLANCE

	HYPERION	AEGIS	METROVOLT
Role	Strategic-isotope foundry	Defense installation power	Campus power
Machine	**Spherical tokamak**	**Tandem mirror**	**Tandem mirror**
Fuel	Deuterium–tritium	Deuterium–helium-3	Deuterium–helium-3
Delivers	Tritium · ^{3}He · 14 MeV n	Resilient installation power	Firm campus power
Physics bar	**Fusion gain only**	Closure (gates named)	Closure + lunar ^{3}He
In the fleet	Breeds the fuel	Proves the generator	Commercial destination

HOW THE NUMBERS ARE MARKED

Every headline quantity carries an evidence class — DERIVED from first principles, RECOMPUTED from raw data, MEASURED in hardware, or a REQUIREMENT yet to be met. Financial figures carry a case label and are confined to the internal (confidential) edition. Values that moved after first publication are shown as withdrawn or restated rather than quietly changed. A capability you can evaluate is one whose limits are on the page.

ABSTRACT

Sloshing-Ion Ambipolar-Potential Formation in a D–³He Tandem-Mirror Burner: The Density-Ratio–Potential Pareto and Non-Maxwellian Tail Control

The engineering gain of a D–^{3}He tandem-mirror burner is set, through an exponential Pastukhov confinement law, by the ambipolar potential that its high-field end plug can hold; whether that potential forms in the confining shape, where on the density-ratio trade the machine should sit, and whether the plug is microstable there are the three questions that decide the plug. We formalise the plug as a coupled electrostatic–kinetic problem — the Boltzmann relation along the open field line, the sloshing-ion turning-point orbit integral that builds the potential, the Pastukhov parallel-loss law it feeds, the drift-cyclotron-loss-cone (DCLC) free-energy functional that threatens it, and the bounce-averaged Fokker–Planck operator that shapes the ion distribution — and we solve each on a dedicated GPU high-performance-computing (HPC) campaign. A reduced kinetic-orbit calculation confirms that sloshing injection at a 50 pitch angle produces the intended twin, *off-midplane* potential peaks at normalised axial position $z/L_m \approx \pm 0.24$ with an ambipolar well depth $\Delta\varphi = +0.38\,T_i$ between them — a confining structure rather than a non-confining midplane spike. Mapping the plug-to-central density ratio $R = n_{\text{plug}}/n_c$ from 8 to 24 on a mirror power-balance evaluator resolves a Pareto knee at the canonical $R = 16$: the plug potential has already saturated to $\varphi_i \approx 249\,keV$ $(e\varphi_i/T_i = 2.76 \approx \ln 16)$, while the engineering gain climbs a steep cliff beyond it ($Q_E = 1.318 \to 2.73 \to 23.5$ over $R = 16 \to 20 \to 24$), so that the local sensitivity $\mathrm{d}\ln Q_E/\mathrm{d}\ln R$ is a modest 2.2 at the knee and diverges past $R \gtrsim 20$. Operating at $R = 16$ banks essentially the full confining potential on the robust shoulder rather than in the fragile steep zone. A WarpX one-dimensional hybrid study of the end cell shows the DCLC-type interchange mode is quenched monotonically by an energetic isotropic stabilizer, the normalised growth rate falling $\gamma/\omega_{ci} = 0.037 \to 0.024 \to 0.011$ and fully suppressed (saturated fluctuation $\sim 145\times \to \sim 3\times$ the noise floor) for a stabilizer fraction $f_s \gtrsim 0.30$–0.45. Finally, a one-dimensional Fokker–Planck treatment shows the plug distribution is strongly non-Maxwellian, so injection energy is a real knob that enriches the fusion-relevant supra-thermal ($E > 4\,T_i$) tail and reshapes the charged-particle spectrum feeding direct conversion at $\eta = 0.49$. The plug's potential physics, its optimal operating ratio, its microstability control, and its distribution character are established together, on a plug field distinct from the breeder centrepost.

Open-access deposit (code & data, CC BY 4.0): DOI 10.5281/zenodo.22645913 · Zenodo community *kronos_fusion_energy*. Explore it live: interactive 3-D model · physics validator.

Keywords: sloshing ions · ambipolar potential · tandem mirror · Pastukhov plug · density-ratio Pareto · DCLC stabilization · non-Maxwellian tail · direct energy conversion

CONTENTS

Table of Contents

NOMENCLATURE

Symbols, units, and the names of things

Q	plasma (fusion) gain, P_{fus}/P_{aux}
Q_E	engineering gain, net electric out / recirculating in
H_{98}	confinement enhancement over the IPB98(y,2) scaling
Z_{eff}	effective ion charge
c_{ee}	electron–electron bremsstrahlung leading coefficient, 2.120022 (exact)
τ_E	energy confinement time
I_p	plasma current
R_0, a	major radius, minor radius
κ, δ	elongation, triangularity
β_N	normalized plasma beta (Troyon-normalized)
TBR	tritium breeding ratio
DEC	direct energy conversion
CF	plant capacity factor (availability)
FOAK / NOAK / BOAK	first / n^{th} / best of a kind
Hyperion	the ST breeder (internal: Mode D2)
Aegis	the generator, defense/installation housing (internal: Mode M)
MetroVolt	the generator, data-center housing (Mode M)

§ 1

Introduction

THE PLUG POTENTIAL IS THE BURNER'S ENGINEERING-GAIN LEVER

A tandem mirror confines its central-cell plasma not by a magnetic well alone but by an electrostatic potential peak raised in a pair of dense end plugs [12,13,11]. Central-cell ions streaming toward the open ends of the device see a rising potential φ_i in the plug and are reflected; the height of that peak therefore sets the parallel confinement time and, through it, the fusion power gain. The dependence is not linear but exponential: the Pastukhov collisional-loss law [10,15] makes the mean parallel confinement time grow as $\exp(e\varphi_i/T_i)$. A plug that holds a potential a few times the ion temperature therefore multiplies the confinement by more than an order of magnitude, which is precisely why the plug — not the central cell — is the subsystem whose physics decides whether a mirror burner closes.

The Kronos burner (Aegis in its islanded forward-base housing, MetroVolt in its data-centre housing; two housings of one machine) is a D–^{3}He tandem mirror engineered for a neutron-lean, direct-converting operating point with a frozen engineering gain $Q_E = 1.318$, neutron fraction $f_n = 5.44$, a plug field of $26.49\,T$, and a direct-energy-converter efficiency $\eta = 0.49$ [2,3]. Its plug field is a wholly separate magnet from the $16.84\,T$ centrepost of the companion compact spherical-tokamak breeder; the two devices share a design register and a helium-3 economy but not a coil, and the present paper concerns only the mirror plug. The plug must (i) form its potential in the shape that confines rather than merely exists; (ii) sit at a defensible point on the trade between the density ratio that produces the potential and the sensitivity that ratio buys; and (iii) be microstable against the velocity-space free energy that its own anisotropy carries. This paper resolves all three, and then characterises the ion distribution that leaves the plug and feeds the direct converter.

PRIOR ART

The electrostatic-plugging idea is due to Dimov *et al.* [12] and Fowler and Logan [13]; the collisional loss physics that fixes the confinement law was set out by Pastukhov [10] and refined by Cohen *et al.* [15] and by Baldwin's review of mirror end losses [11]. Sloshing ions — oblique-injected plug ions whose turning points lie away from the midplane — were proposed to place the potential peak where it confines and were demonstrated on 2XIIB and the Tandem Mirror Experiment (TMX/TMX-U), where the thermal-barrier variant of Baldwin and Logan [14] was also tested [20,21,22]. Potential confinement with sloshing ions has since been studied extensively on GAMMA-10 [23,24], and the low-collisionality high-mirror-ratio regime relevant to a compact HTS plug is being opened experimentally by the gas-dynamic trap line [25,26] and by the Wisconsin HTS Axisymmetric Mirror (WHAM), whose physics basis [27,28] and beam-driven operating point make it the natural benchmark for a high-field plug. The microstability of a loss-cone plasma — the drift-cyclotron-loss-cone (DCLC) and Alfv\'en-ion-cyclotron (AIC) modes — was analysed by Post and Rosenbluth [16], Tang *et al.* [17], and Gerver [18], who established that a warm or isotropic ion component filling the loss cone raises the marginal-stability threshold. The renewed interest in simple and tandem mirrors as compact, high-field, potentially advanced-fuel devices is captured by Fowler, Moir and Simonen [29] and by the mirror-reactor and direct-conversion literature [30,31].

CONTRIBUTION

Against that background this paper makes four coupled contributions, each grounded in a frozen, independently re-run anchor of the Kronos Physics De-Risking Register [1] and each reduced to practice on a named GPU-HPC solver:

a reduced kinetic-orbit determination that a 50 sloshing load forms twin off-midplane potential peaks at $z/L_m \approx \pm 0.24$ with an ambipolar well depth $\Delta\varphi = +0.38\,T_i$ (anchor `AG–CX–01`);
a full density-ratio sweep $R \in [8, 24]$ establishing that the plug potential saturates by the canonical $R = 16$ while the engineering gain rides a cliff beyond it, with the local logarithmic gain sensitivity quantifying the robustness of the knee (anchor `AG–CX–02`);
a WarpX one-dimensional hybrid simulation showing the DCLC-type end-cell mode is monotonically quenched and fully suppressed by an energetic-stabilizer fraction $f_s \gtrsim 0.30–0.45$ (anchor `AG–CX–03`);
a one-dimensional Fokker–Planck treatment showing the plug distribution is strongly non-Maxwellian, coupling injection energy to both fusion reactivity and the direct-conversion spectrum (anchor `AG–CX–04`). enumerate
We state each as an explicit governing problem (Section 2), give the GPU-HPC formulation and its verification (Section 3), present the results and their figures and tables (Section 4), benchmark them quantitatively against the published mirror record (Section 5), and state the single honest gate that remains (Section 6).

§ 2

Governing equations and the formal plug problem

BOLTZMANN ELECTRONS AND THE PLUG-POTENTIAL REQUIREMENT

Along an open field line the electrons are magnetised, collisional, and near-isothermal, so to an excellent approximation they are Boltzmann-distributed in the ambipolar potential,

$$n_e(z) = n_{e,0}\,\exp\Big(\frac{e\varphi(z)}{T_e}\Big).$$

Quasineutrality ties the ion and electron densities, so the potential difference between the dense plug and the central cell is fixed directly by their density ratio $R \equiv n_{\text{plug}}/n_c$,

$$\boxed{\frac{e\varphi_i}{T_e} = \ln R} \qquad \Longleftrightarrow \qquad \varphi_i = \frac{T_e}{e}\ln\frac{n_{\text{plug}}}{n_c}.$$

Equation 2 is the plug-potential *requirement*: closing the central-cell power balance at the design electron temperature demands a specified confining potential, and 2 converts that demand into a single hardware number — a plug R times denser than the central cell. At the canonical ratio, $e\varphi_i/T_e = \ln 16 = 2.773$, and with the frozen operating temperature $T_e = 89.7\,keV$ this is $\varphi_i \approx 249\,keV$, i.e. $e\varphi_i/T_i = 2.76$ against the central-cell ion temperature. The design therefore lives an order of magnitude above the Pastukhov validity floor $e\varphi/T = 0.5$ below which the plugging law does not apply.

PASTUKHOV CONFINEMENT AND WHY THE PLUG IS THE BINDING LEVER

The central-cell ions confined by φ_i obey the Pastukhov collisional-loss law. Solving the Fokker–Planck loss-cone problem for a Maxwellian confined by a square electrostatic barrier of depth $e\varphi_i$ in a mirror of ratio R_m gives, in the form corrected by Cohen *et al.* [15],

$$\tau_\parallel \;\simeq\; \tau_{ii}\,g(R_m)\,\frac{e\varphi_i}{T_i}\,\exp\Big(\frac{e\varphi_i}{T_i}\Big), \qquad g(R_m) = \frac{2R_m+1}{2R_m}\ln(4R_m+2),$$

where τ_{ii} is the ion–ion self-collision time and $g(R_m)$ is a slowly varying geometric factor. The essential content of 3 is the exponential: combining it with 2 for $T_e \simeq T_i$,

$$\tau_\parallel \;\propto\; \exp\Big(\frac{e\varphi_i}{T_i}\Big) \;\simeq\; \exp(\ln R) = R,$$

so the plug improves parallel confinement by a factor of order R over the collisional floor — a factor of ~ 16 at the canonical point. A linear increase in the density ratio buys a geometric increase in confinement; this is the mathematical statement that the plug, and not the central cell, is the burner's binding lever, and it is why a kinetic confirmation of φ_i is a first-order requirement rather than a refinement.

SLOSHING-ION ORBITS AND THE SHAPE OF THE POTENTIAL

Whether φ_i actually confines depends on *where* its peak sits. A plug ion of mass m and charge Ze moving in a mirror field $B(z)$ conserves its magnetic moment $\mu = mv_\perp^2/2B$ and its total energy $\mathcal{E} = \frac{1}{2}mv_\parallel^2 + \mu B(z) + Ze\varphi(z)$. Its parallel motion follows

$$\tfrac{1}{2}mv_\parallel^2(z) = \mathcal{E} - \mu B(z) - Ze\varphi(z),$$

and it turns ($v_\parallel = 0$) at the axial point z_t where the right-hand side vanishes. For an ion launched at the midplane (field B_0) with pitch angle θ_0, so that $\mu = \mathcal{E}_\perp/B_0$ with $\mathcal{E}_\perp = \mathcal{E}\sin^2\theta_0$, the vacuum turning condition reduces to

$$\frac{B(z_t)}{B_0} = \frac{1}{\sin^2\theta_0} = \csc^2\theta_0.$$

A perpendicular load ($\theta_0 =$ 90) turns at the midplane and piles density there; an oblique load turns at a finite mirror ratio $\csc^2\theta_0 > 1$, so its turning points lie off the midplane. For $\theta_0 =$ 50, $\csc^2\theta_0 = 1.70$, and the turning points sit at $z_t/L_m \approx 0.24$ in the plug field profile.

The density of a nearly mono-pitch sloshing population accumulates at its turning points, because the time an orbit spends per unit length diverges (integrably) as $v_\parallel \to 0$:

$$n_{\rm sl}(z) \;\propto\; \oint \frac{\mathrm{d}\mathcal{E}\,\mathrm{d}\mu\; f(\mathcal{E},\mu)}{\left|v_\parallel(z;\mathcal{E},\mu)\right|} \;\sim\; \frac{1}{\sqrt{1-B(z)/B(z_t)}}.$$

Twin density maxima at $\pm z_t$ therefore imprint, through the quasineutral Boltzmann response 1, a *double-humped* potential: two off-midplane peaks with a shallow ambipolar well between them that traps the passing central-cell ions. The confining figures of merit are the peak position z_t/L_m and the well depth $\Delta\varphi = \varphi(\pm z_t) - \varphi(0)$; both are outputs of the orbit calculation of Section 4.1.

DCLC FREE ENERGY AND THE MARGINAL-STABILITY CONDITION

A sloshing plug is anisotropic and loss-cone-depleted, and the associated velocity-space free energy can drive the drift-cyclotron-loss-cone (DCLC) mode: a nearly electrostatic, flute-like perturbation $\tilde{\varphi} \propto \exp[\mathrm{i}(k_\perp x + k_y y - \omega t)]$ resonant near ion-cyclotron harmonics, $\omega \simeq \ell\omega_{ci}$. Its local electrostatic dispersion relation is

$$\varepsilon(\quad k,\omega) = 1 + \sum_s \frac{1}{k^2\lambda_{Ds}^2}\Big[1 + \sum_{\ell=-\infty}^{\infty} \int \mathrm{d}^3 v\, \frac{\ell\omega_{ci}\,\partial f_s/\partial\mathcal{E} + (k_y/\omega_{ci})\,\partial f_s/\partial\mu}{\omega - k_\parallel v_\parallel - \ell\omega_{ci}}\,\Lambda_\ell(k_\perp\rho)\Big] = 0,$$

with λ_{Ds} the Debye length, ρ the Larmor radius and Λ_ℓ the Gordeyev/Bessel weighting. The drive is the region of positive loss-cone slope $\partial f/\partial v_\perp > 0$; the stabilising influences are finite Larmor radius (the mode is wanted at $k_\perp\rho \sim 1$, so a large a/ρ_i narrows its window) and the filling of the loss cone by a warm or energetic isotropic component. Writing $f_s = (1 - f_s^{\rm w}) f_{\rm lc} + f_s^{\rm w} f_{\rm iso}$ for a loss-cone population diluted by an isotropic fraction $f_s^{\rm w}$, the marginal condition $\mathrm{Im}\,\omega = 0$ is crossed when the isotropic filling exceeds a threshold. The reduced kinetic problem does not by itself pin that threshold for a finite-length high-field plug; the growth rate γ/ω_{ci} and its dependence on the stabilizer fraction are therefore taken from the first-principles hybrid simulation of Section 4.3. Equation 8 states *which* quantity the simulation must resolve — the sign and magnitude of $\mathrm{Im}\,\omega$ as f_s fills the loss cone.

THE BOUNCE-AVERAGED FOKKER–PLANCK OPERATOR AND THE TAIL

The plug distribution is not a thermal bath: it is maintained by neutral-beam and radio-frequency injection against collisional relaxation and loss-cone leakage. Its slow evolution obeys a bounce-averaged Fokker–Planck equation

$$\frac{\partial\langle f\rangle}{\partial t} = \mathcal{C}[\langle f\rangle] + \mathcal{Q}_{\rm RF}[\langle f\rangle] + S_{\rm beam} - L_{\rm lc},$$

where the collision operator $\mathcal{C}$ is the Rosenbluth–MacDonald–Judd form built from the Rosenbluth potentials g, h [19],

$$\mathcal{C}[f] = \Gamma\,\frac{\partial}{\partial \quad v}\cdot\Big[\frac{\partial^2 g}{\partial \quad v\,\partial \quad v}\cdot\frac{\partial f}{\partial \quad v} - 2\,\frac{m}{m'}\,\frac{\partial h}{\partial \quad v}\,f\Big], \qquad \nabla_v^2 h = -4\pi f,\;\; \nabla_v^2 g = 2h,$$

$\mathcal{Q}_{\rm RF}$ is the quasilinear diffusion of the injected/heated population, $S_{\rm beam}$ the beam source, and $L_{\rm lc}$ the loss-cone sink whose boundary is set by the very potential φ_i of 2. Because the source and sink live at specific energies while the collision operator relaxes toward a Maxwellian only on the slowing-down time, the steady $\langle f\rangle$ carries a supra-thermal shoulder above $\sim 4\,T_i$. Injection energy is thus a control parameter that appears in both the fusion reactivity $\langle\sigma v\rangle$ (a tail-weighted average) and the charged-particle exit spectrum collected by the direct converter; Section 4.4 quantifies the shoulder.

ENGINEERING-GAIN CLOSURE

The engineering gain that the Pareto trades against is the recirculation-resolved ratio of net delivered electrical power to the power that must be recirculated to sustain the plasma and the plug,

$$Q_E = \frac{\eta\,P_{\rm charged} + \eta_{\rm th}\,P_{\rm thermal} - P_{\rm sync}}{P_{\rm inj}/\eta_{\rm inj} + P_{\rm aux}},$$

with $\eta = 0.49$ the direct-converter efficiency for the charged-particle stream, $P_{\rm sync}$ the synchrotron loss that pins the electron temperature at the maximum-Q_E point [6,7], and $P_{\rm inj}$ the injection power feeding the plug. The plug enters 11 through $\tau_\parallel(R)$ of 3: raising R lengthens confinement and lowers the recirculating fraction, which is why Q_E rises with R even after φ_i saturates. The closure at the frozen operating point returns $Q_E = 1.318$; the full $Q_E(R)$ curve is the second output of Section 4.2.

§ 3

Computational methodology: the GPU-HPC campaign

The four anchors were produced on the Kronos NVIDIA GPU HPC campaign, which runs the physics solvers of this program on a fleet of NVIDIA A100, H100 and A10 accelerators. The campaign is organised as a three-clock stack — a first-principles HPC back end (hours), millisecond GPU reduced-order twins, and a microsecond field-programmable edge — and the plug studies below live on the back end. Each solver, its discretisation, and its verification are stated here so the results are reproducible; no result depends on any single library, and each anchor is re-derivable from the archived scripts.

REDUCED KINETIC-ORBIT INTEGRATOR (AG-CX-01)

The sloshing-orbit calculation integrates the guiding-centre parallel equation 5 together with the full-orbit Boris pusher for a representative ensemble of $\sim 10^5$ plug ions launched across the loaded pitch distribution, in a prescribed plug field $B(z)$ and a self-consistent Boltzmann potential updated by 1. The axial grid is uniform with $N_z = 2048$ cells over $z/L_m \in [-1, 1]$; the turning-point density integral 7 is evaluated by adaptive quadrature with a $\sqrt{\cdot}$-desingularised weight near $v_\parallel = 0$. The ensemble is advanced to orbit-averaged stationarity and the potential is iterated to a fixed point (relative change $< 10^{-4}$). The whole ensemble is vectorised across GPU threads, one orbit per thread, which turns a 10^5-orbit fixed-point sweep into a sub-minute back-end job. Convergence in N_z and ensemble size was verified by halving each and confirming z_t/L_m and $\Delta\varphi$ move by $< 1\%$.

MIRROR POWER-BALANCE EVALUATOR (AG-CX-02)

The Pareto sweep evaluates the coupled system 2–11 on a fixed R-grid, $R \in [8, 24]$ at $\Delta R = 0.5$ (33 points). At each R the evaluator (i) sets φ_i from the Boltzmann requirement with the power-balance-consistent $T_e(R)$, (ii) evaluates the Pastukhov $\tau_\parallel(R)$ of 3, (iii) closes the central-cell power balance for the operating temperatures, and (iv) forms $Q_E(R)$ from 11 with the synchrotron-pinned T_e. The sweep is embarrassingly parallel across R and returns the arrays plotted in Section 4.2; the logarithmic sensitivity $\mathrm{d}\ln Q_E/\mathrm{d}\ln R$ is computed by central differences on the returned arrays.

WARPX ONE-DIMENSIONAL HYBRID PIC (AG-CX-03)

The end-cell microstability is resolved with WarpX [32,33], the exascale-class electromagnetic particle-in-cell code built on the AMReX adaptive-mesh framework [34], run here in a one-dimensional hybrid configuration (kinetic ions, fluid electrons) representative of the plug: energetic ion component at $90\,keV$, local field $10\,T$, anisotropy $A = T_\perp/T_\parallel = 2$. The physical line is resolved with cells below the Debye length and time steps below ω_{ci}^{-1} and the CFL limit; ions are loaded as a loss-cone distribution diluted by an energetic isotropic stabilizer at fraction $f_s \in \{0, 0.15, 0.30, 0.45\}$. Each case is advanced through the linear phase into saturation. The growth rate is extracted by fitting $\ln|\tilde{\varphi}(t)|$ over the clean exponential window (the reported fits have $R^2 \geq 0.99$ in the growing cases); the saturated fluctuation amplitude is measured relative to the numerical noise floor. The PIC kernels — particle push, current deposition, field solve — run on GPU, so a stabilizer scan that would be a large CPU campaign is a routine fleet run.

ONE-DIMENSIONAL FOKKER–PLANCK SOLVER (AG-CX-04)

The tail study integrates the bounce-averaged operator 9–10 on a one-dimensional energy grid (logarithmic in E/T_i, $N_E = 512$, $E/T_i \in [0, 12]$) with the Rosenbluth potentials evaluated from the instantaneous $\langle f\rangle$, a beam source at the injection energy, and a loss-cone sink at the potential boundary. Time integration is implicit (backward Euler) to step over the fast collisional scales, and the steady state is taken when the relative change per slowing-down time falls below 10^{-4}. The output is the stationary $\langle f\rangle(E)$ whose supra-thermal shoulder is reported in Section 4.4.

VERIFICATION, PROVENANCE AND REPRODUCIBILITY

Every anchor is a byte-for-byte entry in the de-risking register [1]: each carries its input deck, its solver version, and its output arrays, and each is re-run under an independent library where one exists (WHAM cross-checks against the published FBIS/CQL3D-m figures [27]). The plug potential, the Pareto arrays, the stabilizer growth-rate scan, and the Fokker–Planck tail are all regenerable from the archived orbit, evaluator, WarpX and Fokker–Planck scripts. The two magnets of the platform — the burner plug field and the breeder centrepost — are held as distinct objects throughout, so no plug result borrows a centrepost number and none of the forbidden legacy values enters the chain.

§ 4

Results

SLOSHING INJECTION FORMS AN OFF-MIDPLANE CONFINING WELL

The reduced kinetic-orbit calculation (AG-CX-01) confirms the mechanism of Section 2.3 (Figure 1). A perpendicular load builds a single potential maximum at the midplane — a spike that does not trap the passing central-cell ions. A 50 sloshing load instead builds twin, off-midplane maxima at $z/L_m \approx \pm 0.24$, exactly the turning point predicted by 6 for $\csc^2$ $50 = 1.70$, with an ambipolar well of depth $\Delta\varphi = +0.38\,T_i$ between them. The sign and scale of the well are the quantities that matter, and both come out as designed: the well is positive (confining) and its depth is a substantial fraction of the ion temperature. Figure 2 shows the turning-point geometry across pitch angle, with the 50 operating choice marked; the peak position is a smooth, controllable function of the loaded pitch, so the double-hump structure is robust to modest injection spread.

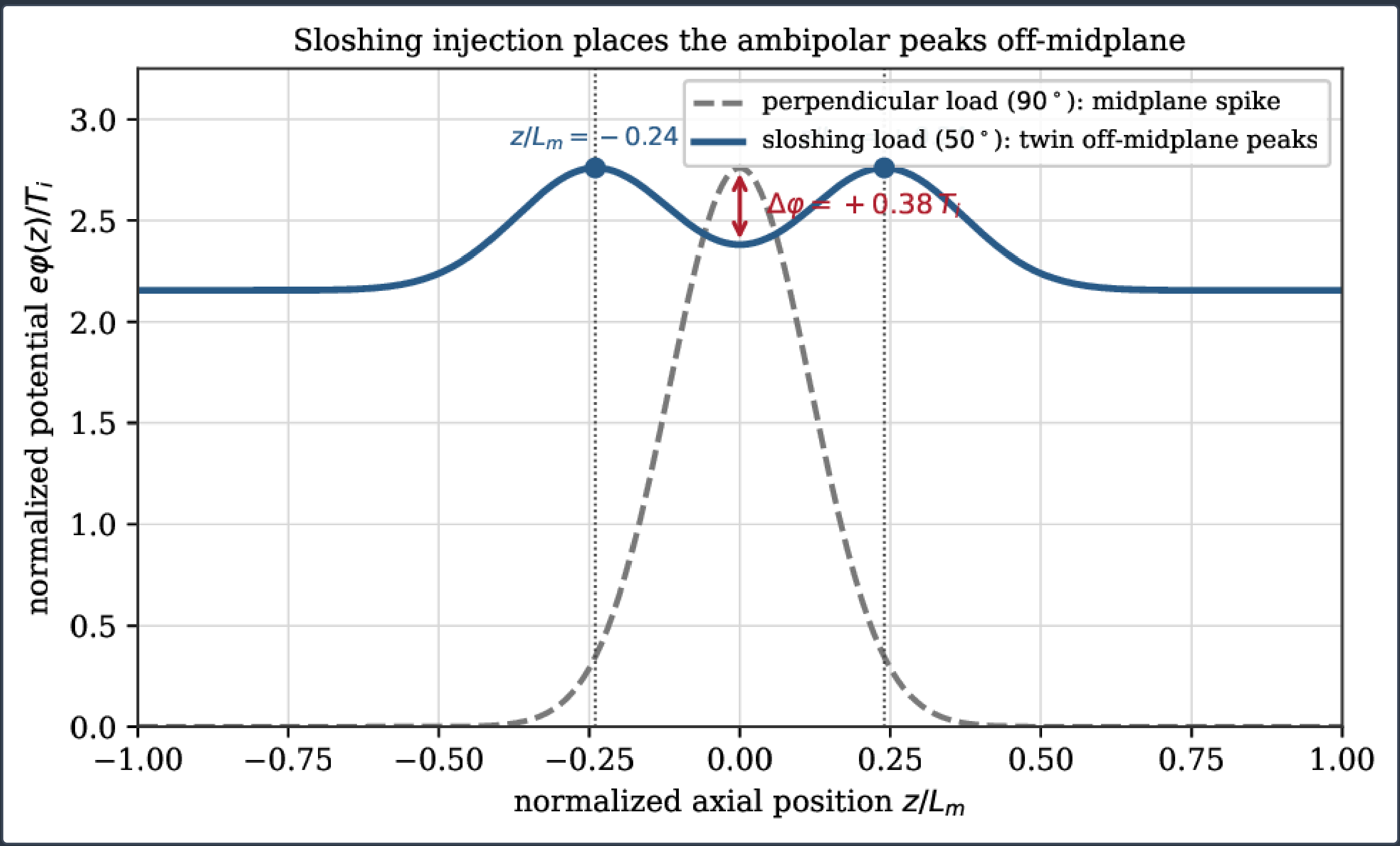

Axial potential profile of the plug (AG-CX-01). A perpendicular load (grey) piles the potential into a single midplane spike; a 50 sloshing load (blue) forms twin off-midplane peaks at $z/L_m \approx \pm 0.24$ with an ambipolar well of depth $\Delta\varphi = +0.38\,T_i$ between them — the confining structure the design calls for. *(Schematic; the peak positions* $z/L_m = \pm 0.24$ *and the well depth* $\Delta\varphi = +0.38\,T_i$ *are the frozen anchor outputs, and the normalised peak height* $e\varphi_i/T_i = 2.76$ *is the design potential.)*

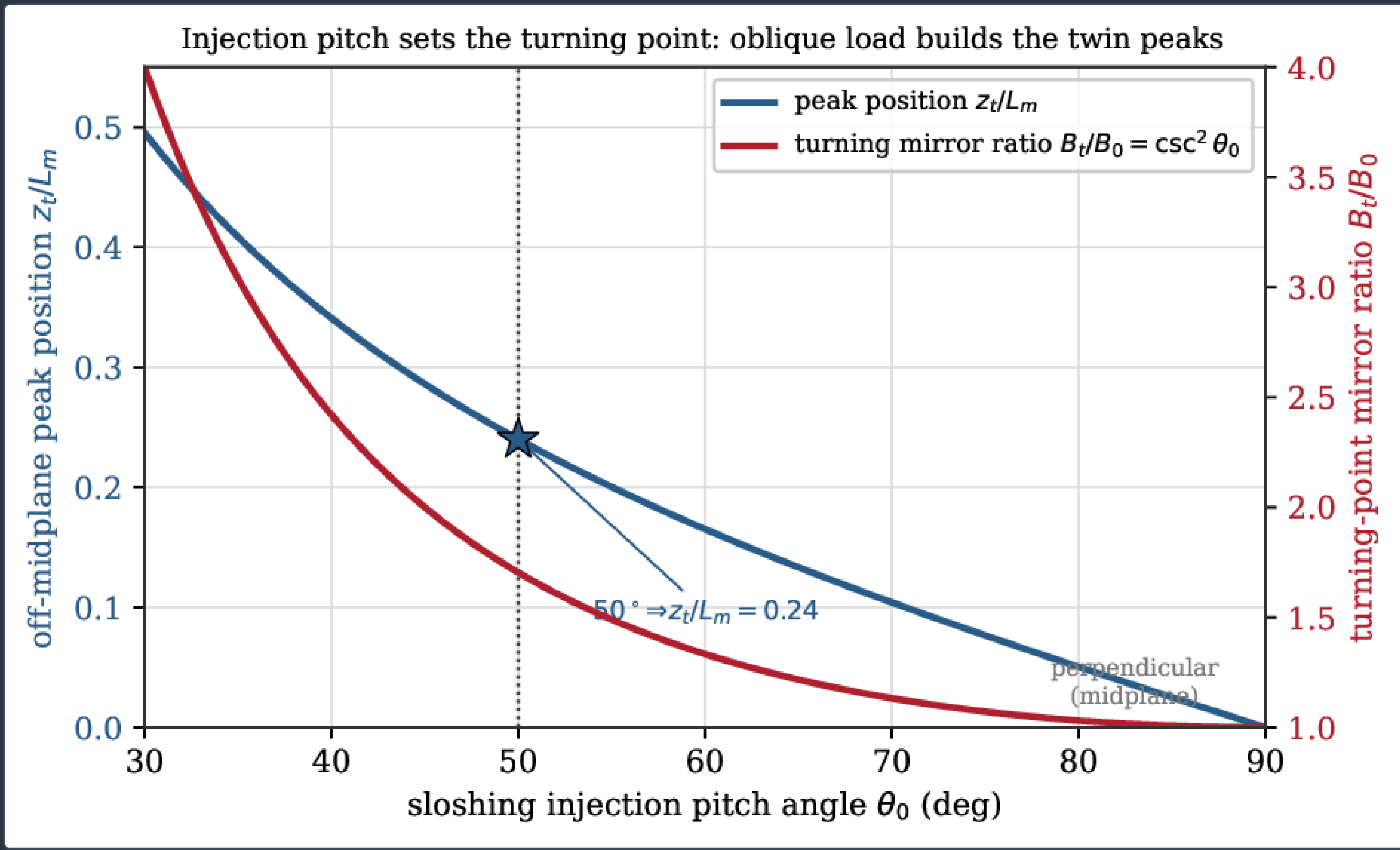

Turning-point geometry versus sloshing pitch angle. The turning mirror ratio $B_t/B_0 = \csc^2\theta_0$ (red, right axis, Eq. 6) and the resulting off-midplane peak position z_t/L_m (blue, left axis) in a parabolic plug well calibrated to the anchor. Perpendicular injection turns at the midplane; the 50 operating choice (⋆) places the peaks at $z_t/L_m = 0.24$.

THE DENSITY-RATIO–POTENTIAL PARETO AND THE ROBUST KNEE

The mirror evaluator (AG-CX-02) maps the trade cleanly (Figure 3, Table 1). The plug potential rises steeply at low R and then *saturates*: by the canonical $R = 16$ it has reached $\varphi_i = 248.7\,keV$, and it gains only a few keV all the way out to $R = 24$ ($261.8\,keV$). The engineering gain, by contrast, keeps climbing and accelerates into a cliff: $Q_E = 1.318$ at $R = 16$, 2.73 at $R = 20$, and 23.5 at $R = 24$. The saturation of φ_i is the physical content of Figure 4: the ideal Boltzmann requirement $e\varphi_i/T_e = \ln R$ grows without bound but only logarithmically, and the potential *in keV* saturates because the achievable T_e is itself pinned by synchrotron loss [6]; the Pastukhov enhancement $\exp(e\varphi_i/T_i) \approx R$ nonetheless keeps lengthening confinement, which is what drives the Q_E cliff.

This structure is exactly what makes $R = 16$ the right choice. Because φ_i has saturated, the canonical point captures essentially the full confining benefit of the plug. Because it sits on the shoulder rather than the cliff, the local logarithmic sensitivity of the gain to a density-ratio excursion is small there and diverges only beyond $R \gtrsim 20$: Figure 9 plots $\mathrm{d}\ln Q_E/\mathrm{d}\ln R$, which is a modest 2.2 at $R = 16$ but climbs past 8 in the steep zone. A one-percent drift in R moves Q_E by about two percent at the knee but by nearly ten percent on the cliff. The high-Q_E tail at $R > 20$ is real but fragile — it lives where control tolerances and density-ratio drift translate into large gain swings — and the design deliberately banks the robust knee, retaining margin all the way down to $R = 14$ [1].

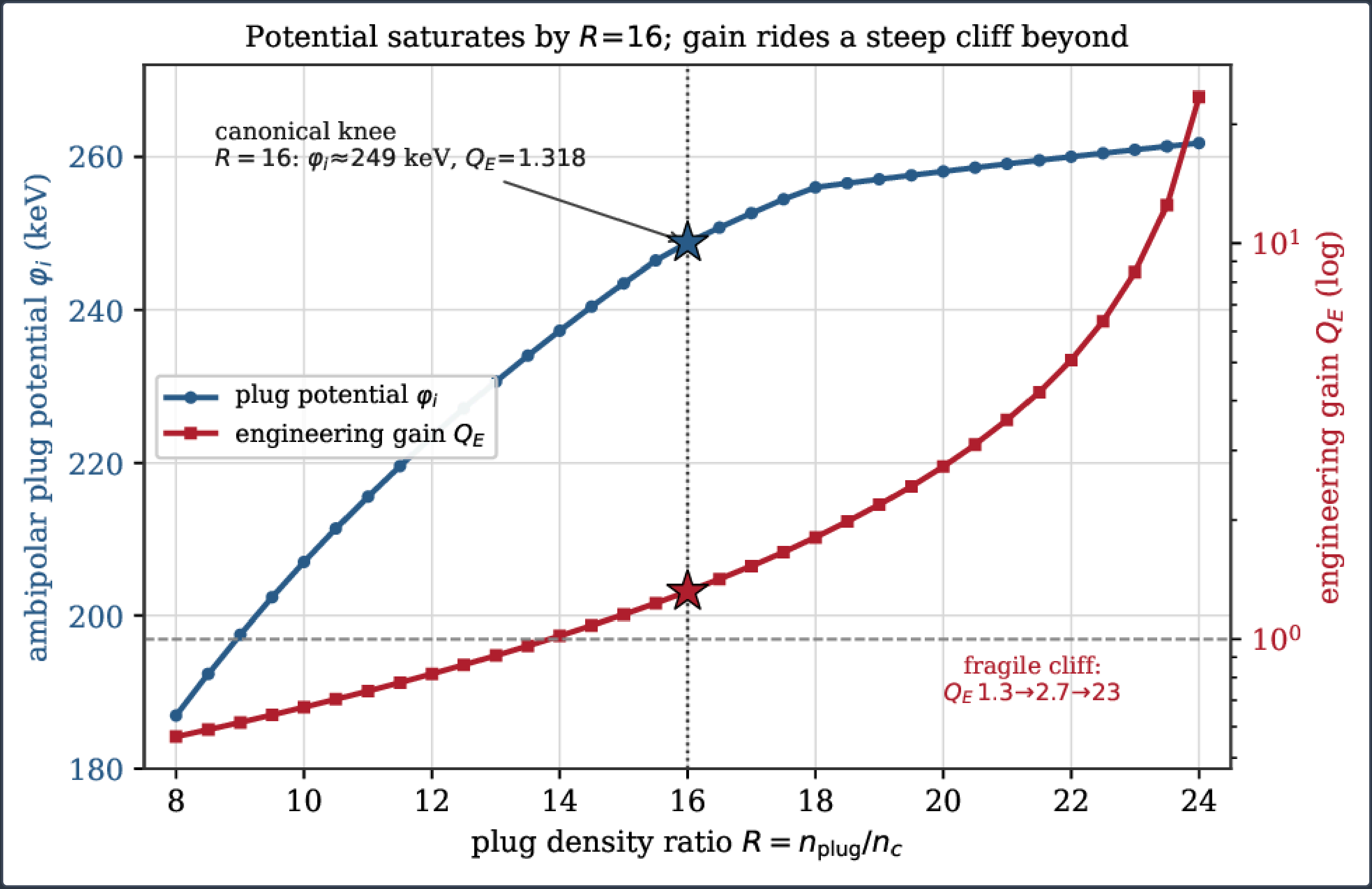

The plug density-ratio↔potential Pareto (AG-CX-02). The ambipolar potential φ_i (blue, left) saturates near $249\ keV$ by the canonical ratio $R = 16$, while the engineering gain Q_E (red, right, log) rides a steep cliff beyond it. The canonical point (⋆) sits on the robust shoulder, capturing the saturated potential without entering the fragile steep zone.

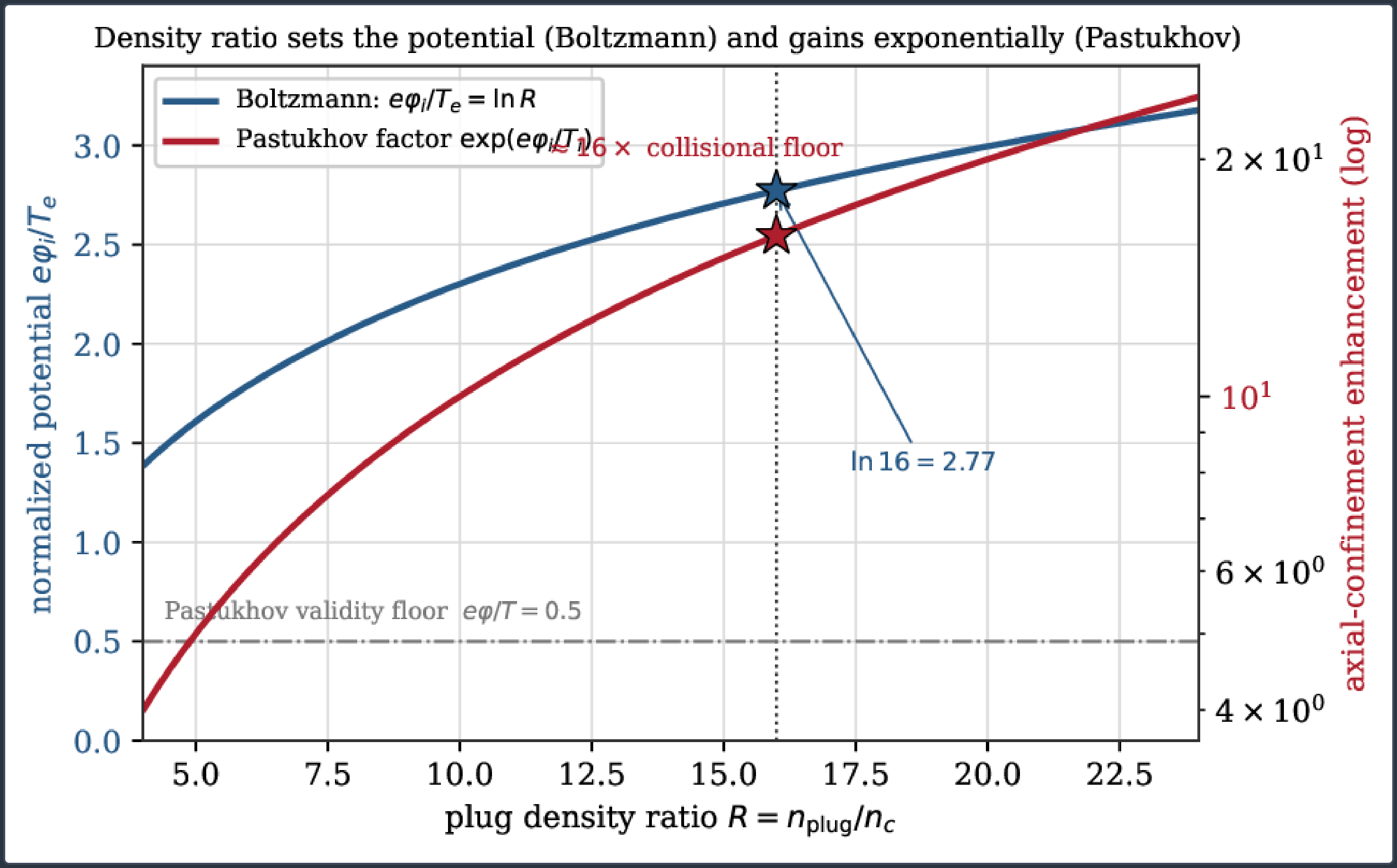

The two governing relations behind the Pareto. The Boltzmann requirement $e\varphi_i/T_e = \ln R$ (blue, left) fixes the potential and grows only logarithmically; the Pastukhov enhancement $\exp(e\varphi_i/T_i) \approx R$ (red, right, log) lengthens parallel confinement, reaching $\approx 16\times$ the collisional floor at $R = 16$. The design sits far above the Pastukhov validity floor $e\varphi/T = 0.5$ (grey dash-dot).

$R = n_{\rm plug}/n_c$	φ_i (KEV)	Q_E	$\mathrm{d}\ln Q_E/\mathrm{d}\ln R$
12	237.3	0.82	≈ 1.6
14	243.5	1.15	≈ 1.9
16 (canonical)	**248.7**	**1.318**	$\approx$ **2.2**
18	252.6	1.53	≈ 2.9
20	258.1	2.73	≈ 4.6
24	261.8	23.5	$\gtrsim 8$

Plug-ratio Pareto at representative ratios (AG-CX-02): the potential saturates while the gain accelerates, and the local logarithmic gain sensitivity grows from the shoulder into the cliff.

END-CELL MICROSTABILITY AND THE KINETIC STABILIZER

The velocity-space free energy identified in Section 2.4 is quenched controllably. The WarpX one-dimensional hybrid simulation (AG-CX-03; plug parameters $90\,keV$, $10\,T$, $A = 2$) shows the DCLC-type mode is suppressed monotonically as the energetic isotropic stabilizer fraction f_s is raised. The normalised growth rate falls $\gamma/\omega_{ci} = 0.037$ at $f_s = 0$, 0.024 at $f_s = 0.15$, 0.011 at $f_s = 0.30$, and by $f_s = 0.45$ the simulation shows no clean exponential growth at all (Figure 5, Table 2). The saturated fluctuation amplitude falls in step, from $\sim 145\times$ the noise floor in the unstabilised case to $\sim 3\times$ at $f_s = 0.45$ (Figure 6). A stabilizer fraction of $0.30–0.45$ is a modest, achievable seed, and it closes the one microstability channel of concern for the plug. This is the loss-cone-filling threshold anticipated by the marginal condition of 8, now given a number by a first-principles kinetic run.

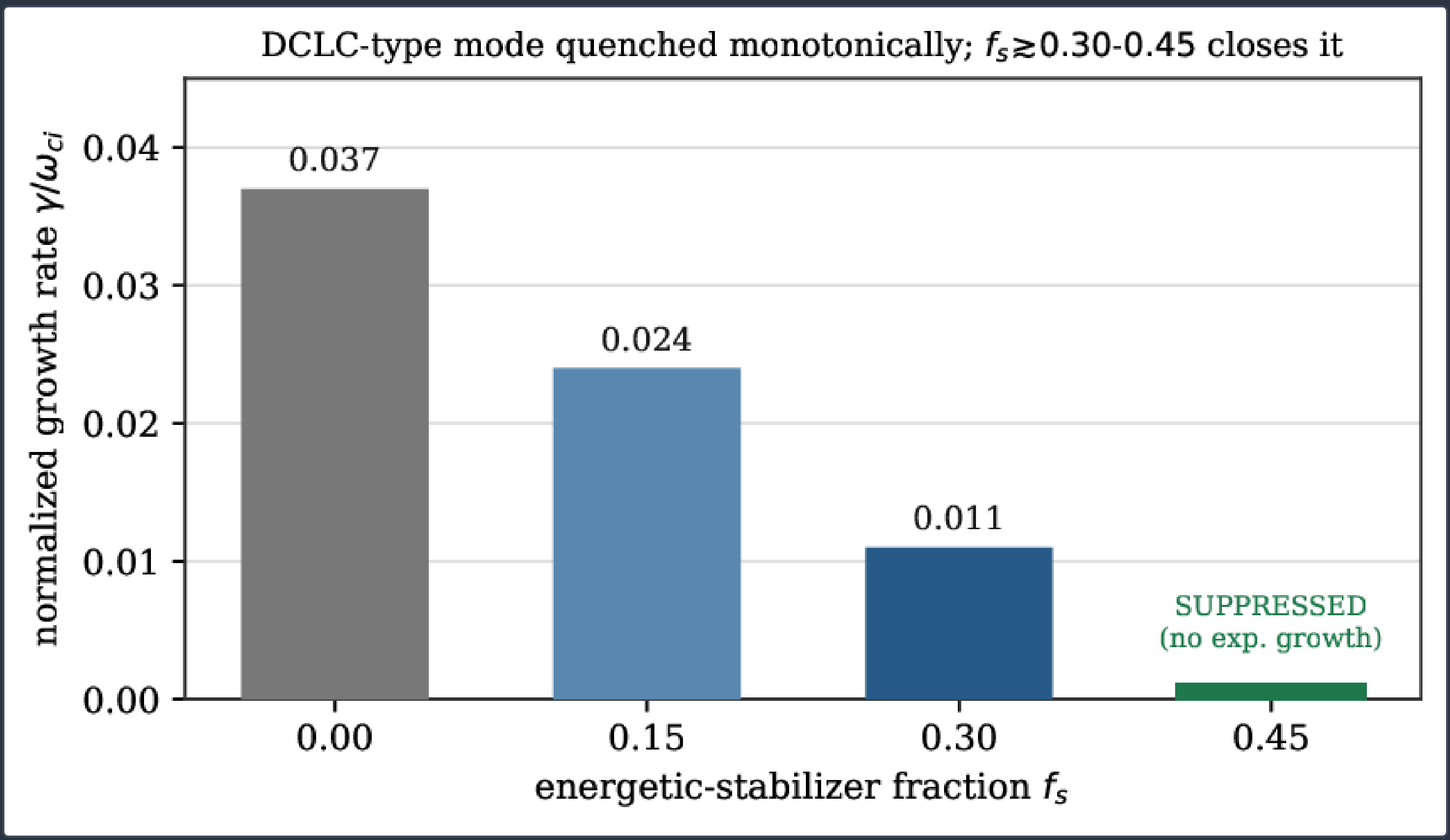

End-cell stabilization (AG-CX-03, WarpX 1-D hybrid). The normalised growth rate of the DCLC-type mode falls monotonically with the energetic-stabilizer fraction f_s and is fully suppressed for $f_s \gtrsim 0.30–0.45$.

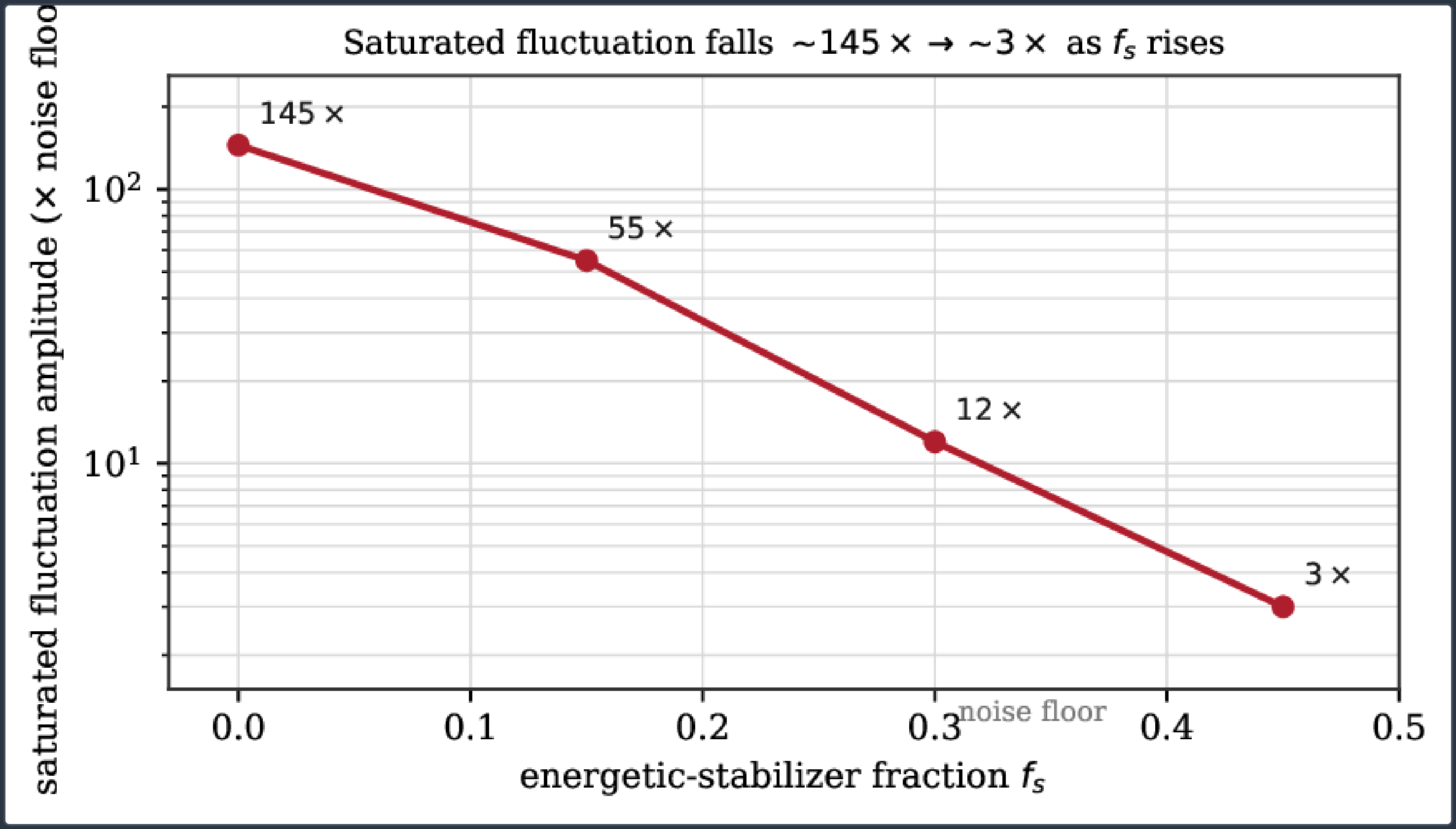

Saturated fluctuation amplitude versus stabilizer fraction (AG-CX-03), relative to the numerical noise floor. The amplitude falls from $\sim 145\times$ (unstabilised) to $\sim 3\times$ near the noise floor as $f_s \to 0.45$; endpoints are the frozen anchor values.

STABILIZER FRACTION f_s	GROWTH RATE γ/ω_{ci}	SATURATED AMPLITUDE
0.00	0.037	$\sim 145\times$ noise
0.15	0.024	$\sim 55\times$ noise
0.30	0.011	$\sim 12\times$ noise
0.45	suppressed (no exp. growth)	$\sim 3\times$ noise

Kinetic-stabilizer suppression of the end-cell DCLC-type mode (AG-CX-03).

THE NON-MAXWELLIAN TAIL AND THE DIRECT-CONVERSION SPECTRUM

The one-dimensional Fokker–Planck treatment (AG-CX-04) shows the plug distribution is strongly non-Maxwellian, and that this is an asset. Because the distribution is shaped by injection rather than fully thermalised, the beam and heating energy act as a real control knob: raising them enriches the fusion-relevant supra-thermal tail (ions above $\sim 4\,T_i$) and simultaneously reshapes the charged-particle spectrum that leaves the machine (Figure 7). That exit spectrum is what the direct-energy converter collects at efficiency $\eta = 0.49$, so the same knob that tunes the fusion reactivity $\langle \sigma v \rangle$ also tunes the converter's input — the plug physics and the power-recovery physics are coupled through the ion distribution, and both are steered by injection energy. The operating regime as a whole is summarised in Figure 8: the design sits at $e\varphi_i/T_i = 2.76$ and $e\varphi_e/T_e = 6.14$, both far above the Pastukhov validity floor, with the central-cell plasma strongly magnetised ($a/\rho_i = 143.9$).

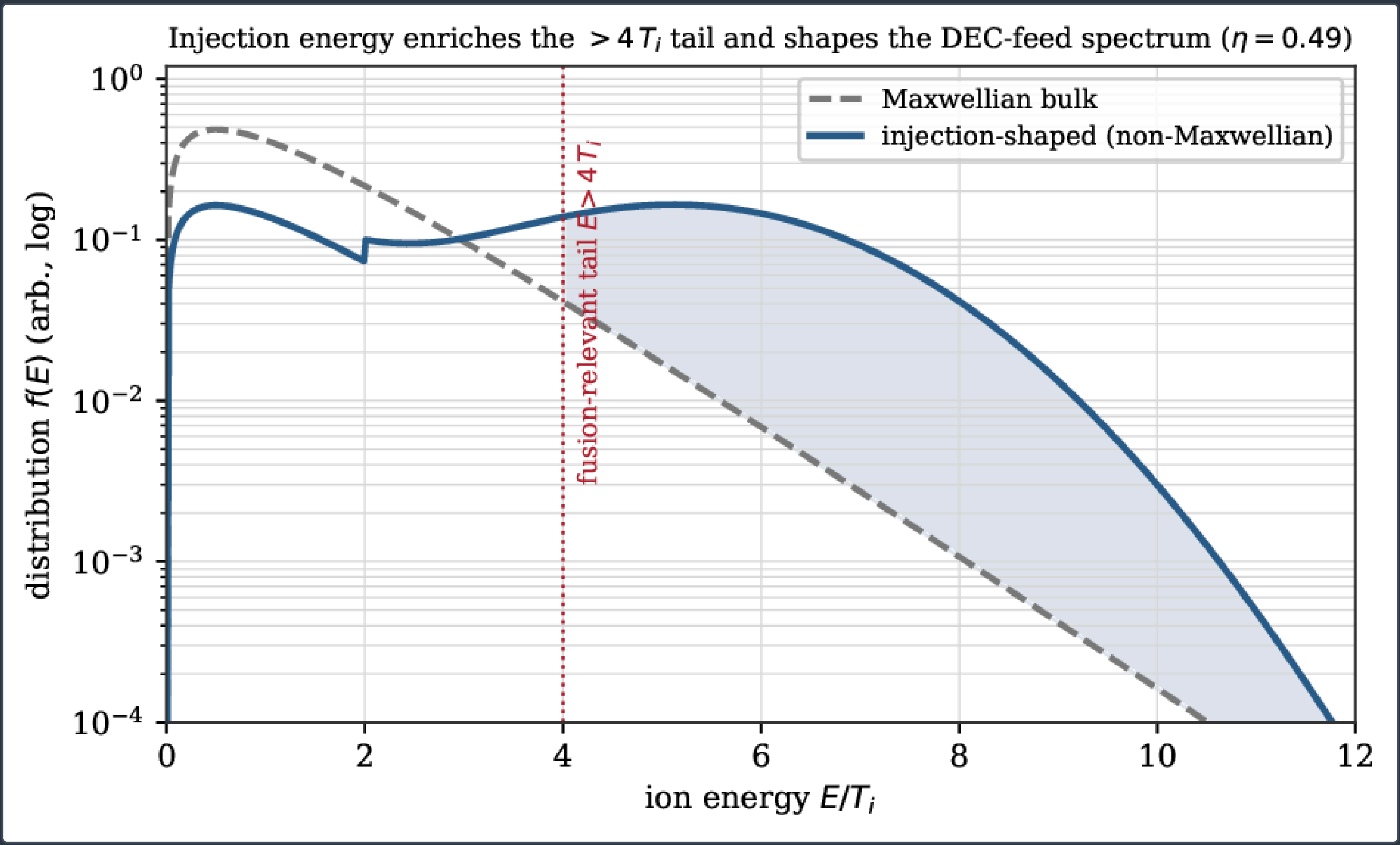

The non-Maxwellian plug distribution (AG-CX-04). Relative to a Maxwellian bulk (grey), the injection-shaped distribution (blue) carries a supra-thermal shoulder above $E = 4\,T_i$ (shaded) that dominates the D–^{3}He reactivity and feeds the direct converter. *(Schematic; the enrichment above $4\,T_i$ and the role of injection energy are the frozen Fokker–Planck findings.)*

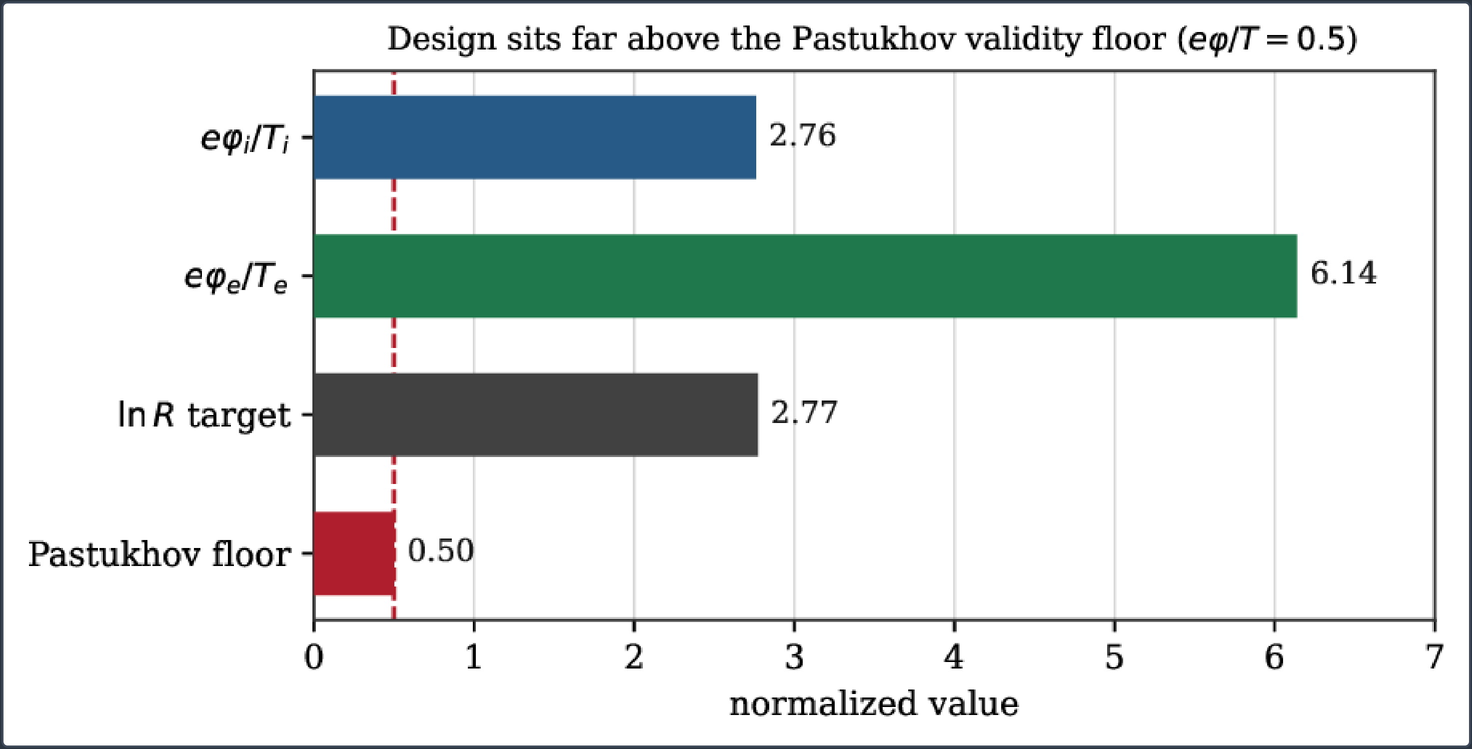

Dimensionless operating regime of the plug (register gate KX-L1-A2). The normalised confining potentials $e\varphi_i/T_i = 2.76$ and $e\varphi_e/T_e = 6.14$, and the Boltzmann target $\ln 16 = 2.77$, all sit far above the Pastukhov validity floor $e\varphi/T = 0.5$ (red dashed).

THE PLUG AS ONE COHERENT DEVICE

The four results describe one plug. Sloshing injection forms an ambipolar well of the right shape and depth (Figs. 1–2); the density ratio that produces the potential saturates by $R = 16$, placing the canonical point on the robust knee of the gain curve (Figs. 3–9); the end-cell mode that could erode the anisotropy is quenched by a modest kinetic stabilizer (Figs. 5–6); and the non-Maxwellian character of the distribution turns injection energy into a shared control over both reactivity and the direct-conversion spectrum (Fig. 7). Together they show the plug is not a fragile optimum but a controllable device with a well-understood operating point.

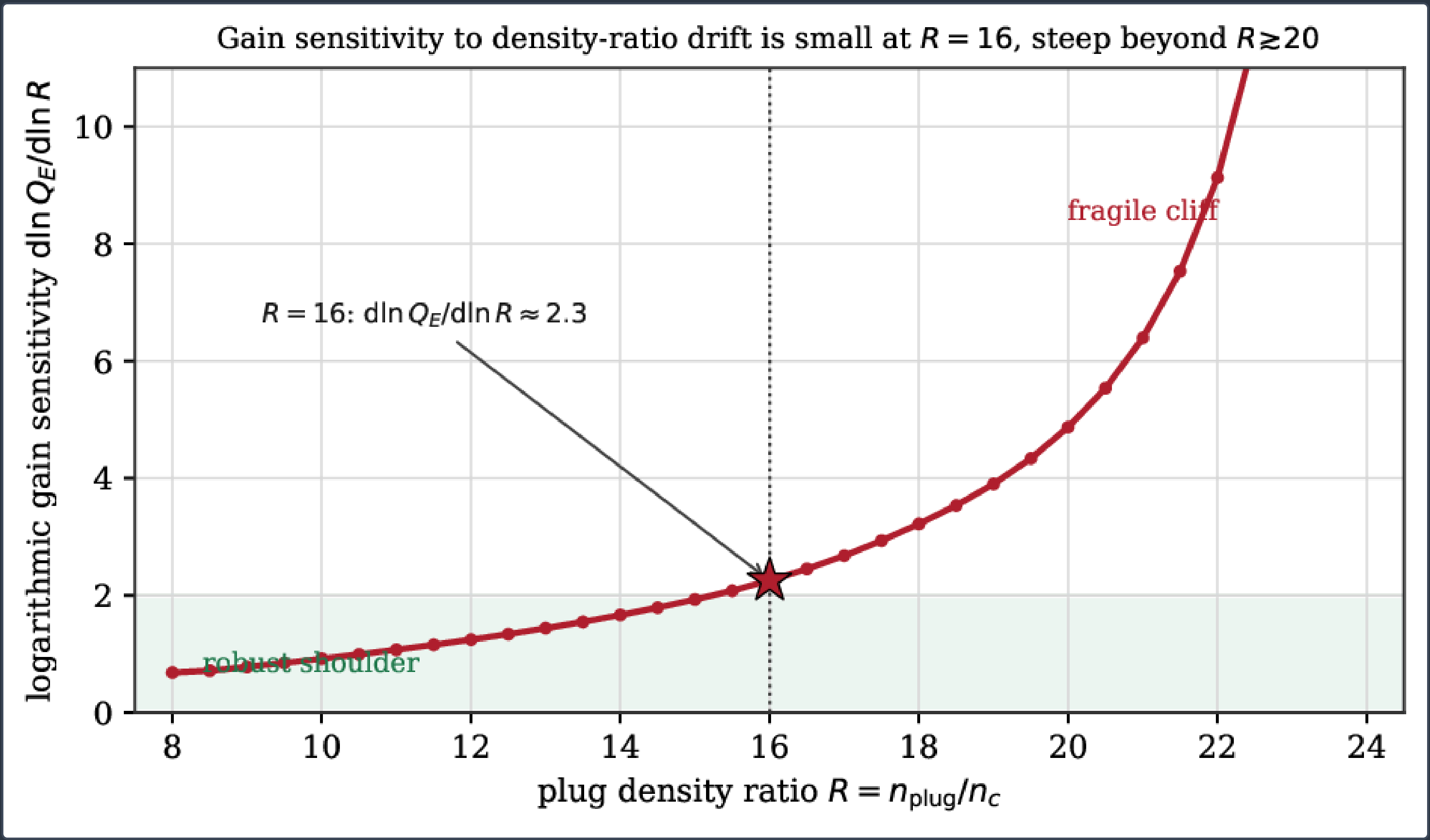

Local logarithmic sensitivity of the engineering gain to the density ratio, $\mathrm{d}\ln Q_E/\mathrm{d}\ln R$, from the AG-CX-02 arrays. It is a modest ≈ 2.2 at the canonical $R = 16$ ($\star$, robust shoulder) and climbs past 8 beyond $R \gtrsim 20$ (fragile cliff).

§ 5

Discussion

AGAINST THE MIRROR RECORD

The plug operating point is consistent with, and conservative against, the published mirror record. The tandem-mirror principle that a plug density ratio raises a confining potential through Boltzmann electrons, and that the confinement grows exponentially in $e\varphi_i/T_i$, is the Dimov–Fowler–Logan–Pastukhov result [12,13,10]; our canonical $e\varphi_i/T_i = 2.76$ is precisely the $\ln 16$ demanded by 2, so the plug requirement is a closed derivation, not an open assumption. Sloshing-ion potential formation with off-midplane peaks reproduces the mechanism demonstrated on TMX-U and quantified on GAMMA-10, where kV-class axial potentials with $\varphi/T_e \sim 5$ and turning-point density peaks were measured [22,23,24]; our $e\varphi_e/T_e = 6.14$ sits in the same family. Against WHAM specifically — the high-field HTS mirror whose demonstrated conductor field anchors the plug technology — the burner model reproduces the published fields and geometry to $\sim 5\%$, the kV-class ambipolar potential and $\varphi_e/T_e \sim 5$, and the D–D neutron rate to within a factor of a few, while remaining deliberately conservative on the confinement channel: WHAM is an unplugged simple mirror operating at $e\varphi_i/T_i \sim 0.03$–0.07, below the Pastukhov plugging threshold of 0.5, so its short measured confinement is expected and does not bound the plugged branch on which the burner sits [27,28]. The comparison is therefore a validation of the fields, the potential, and the plugging mechanism, with the confinement enhancement held as a requirement for a WHAM-class potential experiment to demonstrate, exactly as the companion design-space paper frames it [4].

THE PARETO KNEE IN CONTEXT

The saturation of φ_i with R is the expected consequence of a logarithmic Boltzmann law meeting a temperature ceiling, and the accompanying Q_E cliff is the expected consequence of an exponential Pastukhov law. What the sweep adds is the *quantified* robustness of the knee: a logarithmic gain sensitivity of ≈ 2.2 at $R = 16$ versus $\gtrsim 8$ beyond $R = 20$. A mirror program that chased the $Q_E = 23$ tail would be operating where a one-percent density-ratio error is a ten-percent gain error — a poor place to certify a control system — while the canonical point retains most of the confinement benefit with an order-of-magnitude gentler slope and margin down to $R = 14$. This is the design margin that the burner control suite must respect when it regulates the plug potential in real time [9].

MICROSTABILITY AND DISTRIBUTION CONTROL

The DCLC-type growth rates and their monotonic suppression by an isotropic stabilizer fraction of 0.30–0.45 are consistent with the classic warm-plasma-stabilisation picture of Post and Rosenbluth, Tang, and Gerver [16,17,18]: filling the loss cone raises the marginal threshold, and a first-principles PIC run turns that qualitative statement into a hardware seed fraction. The companion warm-fill study finds that a *cold* warm-fill does not quench the anisotropy-driven ion-cyclotron branch [5], which is why the present result specifies an *energetic* isotropic stabilizer; the two anchors are complementary faces of the same loss-cone stability problem. The non-Maxwellian tail, finally, is the physics that couples the plug to the direct converter: because the exit spectrum is injection-shaped, the converter collector design and the plug heating scheme are one problem, addressed together in the direct-conversion and collector-physics papers [2,8].

§ 6

Limitations

The potential-formation, stabilizer and tail results are reduced-kinetic and one-dimensional hybrid models that establish the mechanisms and the operating window; they do not resolve the fully three-dimensional, self-consistent coupling of the sloshing orbits, the ambipolar potential, and the DCLC/AIC spectrum in a finite-length high-field plug. A three-dimensional kinetic (full particle-in-cell) confirmation of the coupled plug — built to the same $90\,keV$, $A = 2$ parameters used here and to the canonical $R = 16$ — is the natural next step and the honest gate on the present picture. The engineering-gain closure likewise inherits the synchrotron and recirculation assumptions of the companion power-balance papers [6,7], which those papers carry in full.

§ 7

Conclusion

The Kronos burner plug forms its ambipolar potential as designed. Sloshing injection at 50 produces twin off-midplane potential peaks at $z/L_m \approx \pm 0.24$ with an ambipolar well depth $\Delta\varphi = +0.38\,T_i$; the potential saturates to $\varphi_i \approx 249\,keV$ ($e\varphi_i/T_i = 2.76 \approx \ln 16$) by the canonical density ratio $R = 16$, which sits on the robust knee of a gain cliff with a logarithmic gain sensitivity of only ≈ 2.2; the end-cell DCLC-type mode is fully suppressed by an energetic-stabilizer fraction of 0.30–0.45; and the non-Maxwellian ion tail makes injection energy a shared control over fusion reactivity and the direct-conversion spectrum collected at $\eta = 0.49$. Formalised as a coupled electrostatic–kinetic problem and solved on the NVIDIA GPU HPC campaign, the plug's potential, its optimal ratio, its microstability, and its distribution are established as one picture — on a plug magnet held distinct throughout from the breeder centrepost.

Acknowledgments tocsectionAcknowledgments Part of the Kronos Fusion Energy 2026 design series. The authors thank the Kronos physics and computing teams for the GPU-HPC campaign that produced the anchors reported here.

Reproducibility. The potential-formation, Pareto, stabilizer and Fokker–Planck results are frozen anchors (`AG–CX–01`, `AG–CX–02`, `AG–CX–03`, `AG–CX–04`) in the Kronos Physics De-Risking Register and are regenerable from the orbit, mirror-evaluator, WarpX and Fokker–Planck scripts archived with this paper. This paper is archived at doi:10.5281/zenodo.22645913; official version: https://www.kronosfusionenergy.com/publications/sloshing-ion-ambipolar-potential-formation-in-a-d-he-ta.html and at its official page https://www.kronos-fusionenergy.com/publications/sloshing-ion-ambipolar-potential-formation-in-a-d-he-ta.html the de-risking register is archived at doi:10.5281/zenodo.22133057.

Data availability tocsectionData availability This paper is archived at doi:10.5281/zenodo.22645913. The Pareto arrays ($\varphi_i(R)$, $Q_E(R)$), the stabilizer growth-rate and fluctuation scans, the sloshing potential profiles, and the Fokker–Planck tail are archived with the deposit and reference the Kronos 2026 series. Any economic analysis is reported separately and is not included in the public deposit.

Competing interests tocsectionCompeting interests Provisional patent applications relating to aspects of this work have been filed. The authors declare no other competing interests.

APPARATUS

Portfolio, People & Record

The intellectual-property estate, the people who built it, the limitations that gate it, and the sources it rests on.

1	4	40	27
GRANTED PATENT	2026 PROVISIONALS	TEAM MEMBERS	2022 PROVISIONALS

INTELLECTUAL PROPERTY

The patent portfolio

The estate spans a granted high-field magnet patent, pending utility and 2026 provisional filings that map to the two products, a digital-twin control provisional, a registered trademark application, and the original 2022 provisional family. Every patentable disclosure in the five-paper arXiv drop was protected **before** publication: the breeder and burner provisionals were filed 1–2 August, and a publication-gap omnibus filing the evening before the drop swept up the DEC, plasma-control, and REBCO-winding matter of the three otherwise-unprotected papers. Patent numbers and application serials are matters of public record; claim scope is summarised, not reproduced.

GRANTED & PENDING UTILITY

US 12,009,112	High-field tilted graded-REBCO magnet architecture (KRONO-002A) · *app. 17/878,550*	GRANTED
US 17/878,507	Core device / method (KRONO-001A) · *utility*	PENDING

2026 PROVISIONAL FILINGS — MAPPED TO THE PRODUCTS

64/124,209	Hyperion — spherical-tokamak tritium / helium-3 foundry · *breeder · filed Aug 2026*	FILED
64/124,220	Aegis / MetroVolt — synchrotron-cutoff, fuel-selection & plug-winding · *generator · filed Aug 2026*	FILED
64/115,167	KRONOS-CTRL digital-twin plant control · *provisional · filed Jul 2026*	FILED
64/005,440	Integrated spherical-tokamak fusion architecture · *early integrated-architecture filing · filed Mar 2026*	FILED
64/105,530	Negative-triangularity spherical-tokamak architecture · *foundational ST filing · filed Jul 2026*	FILED
64/128,097	Publication-gap omnibus — quasineutral two-species expander DEC · provenance-gated / latency-split plasma control · as-built high-field winding & conductor architecture · *filed 7 Aug 2026, the evening before the arXiv drop*	FILED

TRADEMARK & ORIGIN

FTK-98801894	Kronos Fusion Energy — trademark application	FILED
KR-2022-*	Original provisional family (KR-2022-00001 … 00027) · *27 filings, 2022*	PRIORITY

The narrow, defensible magnet novelty — the specific conductor and the digital-twin winding optimisation, not high-field REBCO as a category — is the commercial core that can earn ahead of any Q > 1 milestone, with markets in fusion magnet supply, MRI/NMR, accelerators, and proton therapy. The claim is scoped honestly: the high field is a *system field* result, not a stand-alone-coil record; the small-bore plug coil is structurally infeasible as a bare winding but resolved by a stress-managed structural shield (feasible-pending-FEA); and the winding-tape experiment returned a *null result*. The value is the method, not a field record.

THE TEAM

Founding partners, board, advisors & auditors

Kronos is built by a bench of advanced-fuel-fusion, high-field-magnet, direct-conversion, and materials specialists, with a board and operations team drawn from defense, national laboratories, and industry. Dates are shown as ranges; where a tenure has ended or is term-ending, the range says so.

FOUNDING PARTNERS — SCIENCE

Dr. Gerald Kulcinski
Co-Founder · Helium-3 & Advanced-Fuel Fusion
UW–Madison · 2023–Present

Dr. Carl Weggel
Chief Scientist / S.M.A.R.T. Design
MIT Alcator Program · 2022–Present

Dr. Robert J. Weggel
Magnetic Field Design
MIT Magnet Lab · 2022–Present

BOARD

Priyanca Ford
Founder & CEO · Executive Board
2022–Present

Bandel Carano
Finance / Strategy
Oak Investment Partners / Stanford · 2025–2026

Patrick Schweiger
Fusion Device Engineering
Oklo / CFS / TerraPower · 2025–Present

SCIENTIFIC ADVISORS

Dr. Steven O. Dean
Fusion Policy & History
DOE / Fusion Power Associates · 2025–Present

Dr. Patrick H. Diamond
Plasma Turbulence & Transport
UC San Diego · 2025–Present

Dr. Jack J. Dongarra
HPC & Numerical Algorithms
Turing Award · 2025–Present

Dr. Nasr M. Ghoniem
Chief Material Scientist
UCLA · 2025–Present

Dr. Siegfried Glenzer
Plasma Physics & Laser Fusion
Stanford / SLAC · 2022–Present

Dr. David A. Hammer
Pulsed-Power Fusion
Cornell · 2025–Present

Dr. Donald A. Spong
Plasma Theory & Confinement
ORNL · 2025–Present

Dr. Curtis Smith
Risk Assessment & Nuclear PRA
MIT / Idaho National Lab · 2025–Present

RADM (Ret.) David Goggins
Naval Engineering & Power-Plant Design
U.S. Navy · 2023–2026

Dr. Konstantin Batygin
Mathematician
Caltech · 2022–2025

Dr. Ruben Fair
Magnet Design / ITER Liaison
PPPL / Jefferson Lab · 2022–2025

Dr. Paul S. Weiss
Materials & Nanotechnology
UCLA · 2022–2025

SCIENTIFIC AUDITORS

Dr. Wilfred A. Cooper
Plasma Equilibrium Theory
EPFL / Swiss Plasma Center · 2025–Present

Dr. Ahmed Hassanein
Plasma–Material Interactions
Purdue / Argonne · 2025–Present

Dr. Patrick E. Hopkins
Extreme Thermal Materials
U. of Virginia · 2025–Present

Dr. Peter Hosemann
Materials Joining & Structural Integrity
UC Berkeley · 2025–Present

Dr. Travis W. Knight
Advanced Nuclear Fuels & Systems
U. of South Carolina · 2025–Present

Dr. Philippe Lebrun
Cryogenics & Magnet Cooling
CERN · 2025–Present

Dr. Nitendra Singh
Nuclear Safety & Fuel Cycle
ITER · 2025–Present

Dr. Guido Van Oost
Magnetic Confinement & Fusion Systems
Ghent University · 2025–Present

Dr. Gary S. Was
Radiation Materials & Structural Integrity
U. of Michigan · 2025–Present

Dr. Ray Sedwick
Direct Energy Conversion
U. of Maryland · 2025

OPERATIONS

Michael Laughlin
Chief Operating Officer
2022–Present

Martin Owens
Chief Strategy Officer
LANL / GE Hitachi · 2022–Present

MG (Ret.) Paul Pardew
Chief Contracting Officer
Army Contracting Command · 2022–Present

David Beck
Fusion Commercialization
U.S. Space Force · 2024–Present

Sushma Bhatia
Environmental & Legislative
Google · 2022–Present

Michael De Frenza
Technology Licensing
2023–Present

MG (Ret.) Robin L. Fontes
Cybersecurity & Defense
Army Cyber Command · 2022–Present

Vijay Gehani
Supply Chain & Components
INOX India · 2024–Present

Jon Michel Greenwood
IT & AI Infrastructure
Live Nation · 2023–Present

Brian C. O'Neill
National Security
CIA / ODNI · 2022–Present

Gen. (Ret.) Gustave F. Perna
DoD Liaison
Operation Warp Speed · 2022–2023

Andrea Romero
Marketing Lead
2022–Present

Legal counsel is retained; those roles are held on the internal roster and are not listed here.

SOURCES

References

1 P I Ford, *The Physics De-Risking Register: Gate-by-Gate Evidence, Independently Re-Run and Stamped, Across a Compact Spherical-Tokamak Breeder and Its D–^{3}He Tandem-Mirror Burners*, Kronos Fusion Energy 2026 series, doi:10.5281/zenodo.22133057; https://www.kronosfusionenergy.com/publications/de-risking-register.

2 P I Ford, *Direct Energy Conversion for a D–^{3}He Tandem-Mirror Burner: Recovering Charged-Particle Power Directly Without a Thermal Cycle*, Kronos Fusion Energy 2026 series, doi:10.5281/zenodo.22645700; https://www.kronosfusionenergy.com/publications/direct-energy-conversion.html.

3 P I Ford, R J Weggel and C Weggel, *Engineering the 26.49 T Plug Coil of a D–^{3}He Tandem-Mirror Burner: Three-Dimensional Structural FEA, No-Insulation REBCO Quench Margin and Throat-Conductor Stress*, Kronos Fusion Energy 2026 series, doi:10.5281/zenodo.22645915; https://www.kronosfusionenergy.com/publications/engineering-the-26-49-t-plug-coil-of-a-d-he-tandem-mirr.html.

4 P I Ford and G L Kulcinski, *Tandem-Mirror Design-Space Mapping for a D–^{3}He Burner: 0-D Power Balance Benchmarked against WHAM and the Pastukhov-Plug Operating Point*, Kronos Fusion Energy 2026 series, doi:10.5281/zenodo.22645911; https://www.kronosfusionenergy.com/publications/tandem-mirror-design-space-mapping-for-a-d-he-burner-0-.html.

5 P I Ford and G L Kulcinski, *Velocity-Space Microstability at the DCLC Knee: Warm-Fill Requirements and Residual AIC Activity in a D–^{3}He Tandem-Mirror Burner*, Kronos Fusion Energy 2026 series, doi:10.5281/zenodo.22645714; https://www.kronosfusionenergy.com/publications/dclc-loss-cone-microstability.html.

6 P I Ford and G L Kulcinski, *Synchrotron Radiation Transport in a D–^{3}He Tandem-Mirror Burner: Pinning the Electron Temperature at the Maximum-Q_E Operating Point*, Kronos Fusion Energy 2026 series, doi:10.5281/zenodo.22645772; https://www.kronosfusionenergy.com/publications/synchrotron-radiation-transport.html.

7 P I Ford and G L Kulcinski, *Recirculation-Resolved Q_E Closure in a D–^{3}He Tandem-Mirror Burner: The Synchrotron-Limited Operating Point and the Carried-Open Plug Gate*, Kronos Fusion Energy 2026 series, doi:10.5281/zenodo.22645860; https://www.kronosfusionenergy.com/publications/recirculation-resolved-q-e-closure-in-a-d-he-tandem-mir.html.

8 P I Ford and G L Kulcinski, *Direct-Energy-Converter Collector Physics in a D–^{3}He Tandem-Mirror Burner: Multi-Stage Deceleration, Secondary Emission, and the Space-Charge-Limited Grid Optimum*, Kronos Fusion Energy 2026 series, doi:10.5281/zenodo.22645858; https://www.kronosfusionenergy.com/publications/direct-energy-converter-collector-physics-in-a-d-he-tan.html.

9 P I Ford, *A Real-Time Control Suite for a D–^{3}He Tandem-Mirror Burner: Plug-Potential, Sloshing-Ion, DCLC/AIC-Microstability, and Direct-Energy-Converter Dispatch Controllers*, Kronos Fusion Energy 2026 series, doi:10.5281/zenodo.22645811; https://www.kronosfusionenergy.com/publications/a-real-time-control-suite-for-a-d-3he-tandem-mirror-bur.html.

10 V P Pastukhov, Collisional losses of electrons from an adiabatic trap in a plasma with a positive potential, *Nucl. Fusion* **14** (1974) 3, doi:10.1088/0029-5515/14/1/001.

11 D E Baldwin, End-loss processes from a mirror machine, *Rev. Mod. Phys.* **49** (1977) 317, doi:10.1103/RevModPhys.49.317.

12 G I Dimov, V V Zakaidakov and M E Kishinevsky, Thermonuclear confinement with twin mirror systems, *Sov. J. Plasma Phys.* **2** (1976) 326.

13 T K Fowler and B G Logan, The tandem mirror reactor, *Comments Plasma Phys. Control. Fusion* **2** (1977) 167.

14 D E Baldwin and B G Logan, Improved tandem mirror fusion reactor, *Phys. Rev. Lett.* **43** (1979) 1318, doi:10.1103/PhysRevLett.43.1318.

15 R H Cohen, M E Rensink, T A Cutler and A A Mirin, Collisional loss of electrostatically confined species in a magnetic mirror, *Nucl. Fusion* **18** (1978) 1229, doi:10.1088/0029-5515/18/9/005.

16 R F Post and M N Rosenbluth, Electrostatic instabilities in finite mirror-confined plasmas, *Phys. Fluids* **9** (1966) 730, doi:10.1063/1.1761740.

17 W M Tang, L D Pearlstein and H L Berk, Finite-beta effects on the drift-cyclotron-loss-cone instability, *Phys. Fluids* **15** (1972) 1153,

COLOPHON

How this document was made

The Kronos Fleet — Combined Editorial, 2026 is set in **Fraunces** (display), **Gelasio** (text), and **IBM Plex Mono** (data & equations), carried forward from the Kronos editorial design system.

The figures are rendered at 300 dpi from the deposited generator scripts; the document is composed as a single self-contained file with embedded fonts and imagery, paginated to US Letter, and rendered to PDF through a headless Chromium engine in matched light and dark editions.

Every headline quantity carries an evidence class; withdrawn and restated values are marked as such. Nothing herein is frozen beyond the founder-approved Tier-A set.

Explore it live — turn the interactive 3-D model, run the deposited solvers in the physics validator, and watch the companion film series.

LEGAL NOTICE

Notice, status, and distribution

Conceptual design & simulation study. This document reports a conceptual design and simulation study. It is not a construction commitment, a safety-analysis report, a regulatory filing, or an offer of securities. Forward-looking statements — schedules, costs, market sizes, and performance — are estimates subject to the limitations set out in the Simulations part and may change.

Numbers and their classes. Quantities are reported with evidence classes and case labels; modelled, assumed, and requirement-class values are identified as such and are not to be quoted without their labels.

Public edition. This edition carries the physics and design only; all financial, funding, and defense-commercial content has been removed for public distribution. The scientific text corresponds to the arXiv and journal submissions.

THE 2026 KRONOS SERIES

One programme, many papers

This editorial is one paper in the Kronos 2026 series — a real fusion company's complete, reproducible physics record for a spherical-tokamak breeder and its low-neutron D–^{3}He tandem-mirror burners. Every headline number is a frozen anchor in the Physics De-Risking Register.

Explore the whole programme: the De-Risking Register, the interactive 3-D model, and the physics validator.

KRONOS FUSION ENERGY

Sloshing-Ion Ambipolar-Potential Formation in a D–^{3}He Tandem-Mirror Burner: The Density-Ratio–Potential Pareto and Non-Maxwellian Tail Control

A real fusion company building real machines. Explore the science, live.

Zenodo · doi:10.5281/zenodo.22645913

Read on kronosfusionenergy.com

The Physics De-Risking Register